

Measurement of jet shapes in top pair events at $\sqrt{s} = 7$ TeV using the ATLAS detector

Javier Llorente, on behalf of the ATLAS Collaboration*

Universidad Autónoma de Madrid

E-mail: javier.llorente.merino@cern.ch

A measurement of jet shapes in top pair events using 1.8 fb^{-1} of $\sqrt{s} = 7$ TeV pp collision data recorded by the ATLAS detector at the LHC is presented. Samples of top pair events are selected in both the single-lepton and dilepton final states. The differential and integrated shapes of the jets initiated by bottom-quarks from the top-quark decays are compared with those of the jets originated by light-quarks from the hadronic W -boson decays $W \rightarrow q\bar{q}'$ in the single-lepton channel. Light-quark jets are found to have a narrower distribution of the momentum flow inside the jet cone than b -quark jets.

*XXI International Workshop on Deep-Inelastic Scattering and Related Subject -DIS2013,
22-26 April 2013
Marseilles, France*

*Speaker.

1. Introduction

Jet shapes [1, 2, 3] provide a way of studying the jet substructure in terms of the energy distribution of the constituents inside the jet cone. Due to the mass of the b -quark, jets originating from a b -quark (b -jets) are expected to be broader than light-quark jets, including charm jets (light jets). This expectation is supported by observations by the CDF collaboration [4], where a comparison is presented between jet shapes in a b -jet enriched sample with a purity of roughly 25% and an inclusive sample where no distinction is made among the flavours.

2. Event selection

Two samples of events are selected: a dilepton sample, where both W bosons decay to leptons (e , μ , including leptonic τ decays), and a single-lepton sample, where one W boson decays to leptons and the other to a $q\bar{q}'$ pair, giving rise to two jets.

The dataset used corresponds to pp collision data with a center-of-mass energy $\sqrt{s} = 7$ TeV and an integrated luminosity of 1.8fb^{-1} . Events are triggered by inclusive high- p_T electron or muon triggers, with an 18 GeV threshold for muons and 20 GeV threshold for electrons.

2.1 Dileptonic sample

The offline selection in the dilepton sample follows that in Ref. [5]. It is done by requiring the events to contain exactly two isolated leptons (e or μ) with transverse momenta $p_T(e) > 25$ GeV and $p_T(\mu) > 20$ GeV. Additionally, the missing transverse momentum is required to be $E_T^{\text{miss}} > 60$ GeV for the ee and $\mu\mu$ channels. For the $e\mu$ channel, H_T is required to be greater than 130 GeV, where H_T is the scalar sum of the p_T of all muons, electrons and jets.

Dilepton events are also required to contain at least two jets, one of which has to be tagged with a 57% efficiency b -tagging algorithm. Finally, the two-lepton invariant mass $m_{\ell\ell}$ is required to be greater than 15 GeV and to satisfy $|m_{\ell\ell} - m_Z| \geq 10$ GeV. The number of selected events in data is 2067. Based on Monte Carlo estimates, 95% of the sample corresponds to $t\bar{t}$ events and the other 5% to a set of backgrounds, dominated by the single-top processes.

2.2 Single-lepton sample

In this case, the selection is done following the steps in Ref. [6]. Events are required to contain exactly one isolated lepton and the missing transverse momentum E_T^{miss} is required to be greater than 35 GeV in the electron channel and greater than 20 GeV in the muon channel. Furthermore, the transverse mass defined as

$$m_T = \sqrt{2p_T^\ell E_T^{\text{miss}}(1 - \cos \Delta\phi_{\ell\nu})} \quad (2.1)$$

is required to be greater than 25 GeV in the e -channel and to satisfy the condition $E_T^{\text{miss}} + m_T > 60$ GeV in the μ -channel.

The jet selection requires at least four jets with the same kinematic conditions as in the dilepton case, one of which is required to be b -tagged. In this case, the total number of selected events in data is 17019. The proportion of $t\bar{t}$ events has been estimated to be 77.4%, the rest being a mixture of background processes, which are dominated by W +jets production at the level of 12.8%.

3. Jet sample definition

Jets in the dilepton and single-lepton channel are subdivided into light-jet and b -jet samples. The contributions from pileup are removed using the JVF algorithm and the p_T threshold of jets is raised to 30 GeV. Also, in order to avoid jet-jet overlaps which would bias the jet shape measurement, any selected jet is required to be separated more than $\Delta R = 0.8$ from any other jet in the event¹. The purity of each jet sample is estimated from Monte Carlo samples for the contributing processes and is defined as

$$p = \sum_k \alpha_k p_k; \quad p_k = 1 - \frac{N_{\text{f}}^{(k)}}{N_{\text{T}}^{(k)}} \quad (3.1)$$

where α_k are the proportions of signal and background processes in the total sample and p_k are the purities in each of these partial samples.

3.1 b -jet samples

To select the b -quark jet candidates in both event samples, a neural-network algorithm is used which mainly relies on the reconstruction of the secondary vertices and the 3D impact parameter information. It has an efficiency of 57% for jets originating from b -quarks in simulated $t\bar{t}$ events, while the rejection factor is about 400 for u, d, s jets and 10 for c -jets [7]. Figure 1 (left) shows the p_T distribution of b -jets in the single-lepton channel.

The purity of the b -jet sample in the dilepton channel has been estimated to be $p_b^{(\text{d})} = (99.3^{+0.7}_{-6.5})\%$, while the b -jet purity for the single-lepton channel is found to be $p_b^{(\text{s})} = (88.5 \pm 5.7)\%$.

3.2 Light jet sample

The hadronic decays of the W boson are a clean source of light-quark jets as gluons and b -quarks are highly suppressed. To select the light-jet sample, the jet pair in the event which has the invariant mass closest to the W -boson mass is selected. Both jets are also required to be non-tagged by the b -tagging algorithm. Figure 1 (right) shows the the invariant mass of the dijet system. Using Eq. 3.1, the purity of the light-jet sample is found to be $p_1^{(\text{s})} = (66.2 \pm 4.1)\%$.

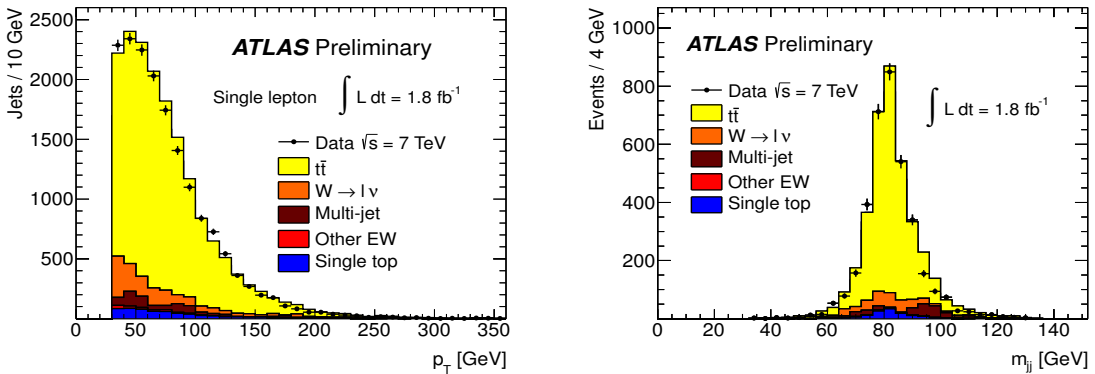


Figure 1: The p_T distribution of b -jets in the single lepton channel (left) and the invariant mass distribution of light-jet pairs (right), along with the sample composition expectations.

¹The distance in the η - ϕ plane is defined as $\Delta R = \sqrt{(\Delta\eta)^2 + (\Delta\phi)^2}$

4. Jet shape definition

Differential $\rho(r)$ (integrated $\Psi(r)$) jet shapes are defined as the fraction of transverse momentum in concentric annuli (circles) centered in the jet axis direction with respect to the total sum of p_T within the jet cone. Here we will concentrate on the average values of the jet shape variables, defined as

$$\langle \rho(r) \rangle = \frac{1}{\Delta r} \frac{1}{N_{\text{jets}}} \sum_{\text{jets}} \frac{p_T(r - \Delta r/2, r + \Delta r/2)}{p_T(0, R)} \quad (4.1)$$

$$\langle \Psi(r) \rangle = \frac{1}{N_{\text{jets}}} \sum_{\text{jets}} \frac{p_T(0, r)}{p_T(0, R)} \quad (4.2)$$

Here, $\Delta r = 0.04$ is the bin width, $\Delta r/2 \leq r \leq R - \Delta r/2$ is the distance to the jet axis in the η - ϕ plane, and $p_T(r_1, r_2)$ is the scalar sum of the p_T of the jet constituents with radii between r_1 and r_2 . Figure 2 shows the values of $\langle \rho(r) \rangle$ and $\langle \Psi(r) \rangle$ as a function of the clustering distance r .

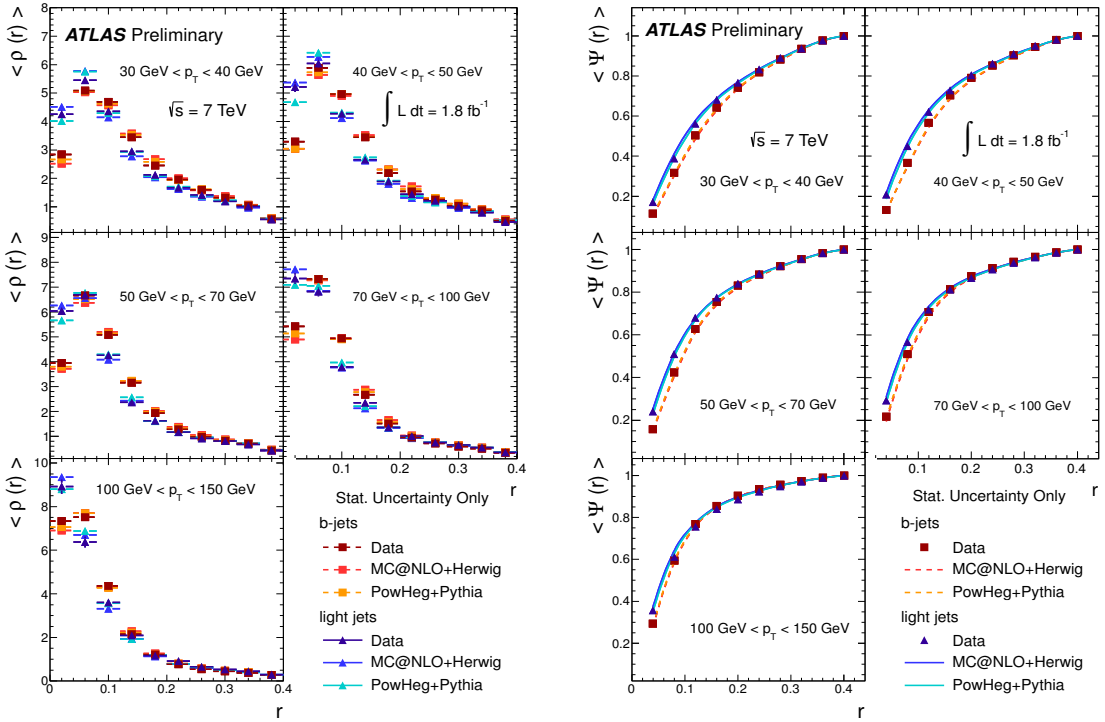


Figure 2: Average values of the differential (left) and integrated (right) jet shapes $\langle \rho(r) \rangle$, $\langle \Psi(r) \rangle$ as a function of r at the detector level, compared to MC@NLO+HERWIG and POWHEG+PYTHIA event generators. The uncertainties shown for data are only statistical.

As expected, the values of $\langle \Psi(r) \rangle$ are greater for light jets than for b -jets, indicating that b -jets have a wider spread of the energy inside the cone. It is also observed that $\langle \Psi(r) \rangle$ increases as the transverse momentum is increased, thus indicating that jets become more collimated with increasing p_T .

5. Unfolding to the particle level

In order to correct the experimental data for detector effects, thus enabling comparisons with MC generators and other experiments, a bin-by-bin unfolding is performed. The particle-level jets are built using all particles with an average lifetime above 10^{-11} s, excluding muons and neutrinos. For particle-level b -jets, a b -hadron with $p_T > 5$ GeV is required to be closer than $\Delta R = 0.3$ from the jet axis, while for light jets, the non- b -jet pair with invariant mass closest to m_W is selected. The same kinematic selection criteria are applied to these particle-level jets as for the reconstructed jets, namely $p_T > 25$ GeV, $|\eta| < 2.5$ and $\Delta R > 0.8$ to avoid jet–jet overlaps. The correction factors are defined as

$$F_{1,b}^\rho(r) = \frac{\langle \rho(r)_{1,b} \rangle_{\text{MC,part}}}{\langle \rho(r)_{1,b} \rangle_{\text{MC,det}}} \quad (5.1)$$

$$F_{1,b}^\Psi(r) = \frac{\langle \Psi(r)_{1,b} \rangle_{\text{MC,part}}}{\langle \Psi(r)_{1,b} \rangle_{\text{MC,det}}} \quad (5.2)$$

The experimental data is then corrected by multiplying the bin-by-bin values by these factors.

6. Systematic uncertainties

The main sources of systematic uncertainties are summarized in table 1. The greater contributions come from the cluster energy scale, pileup and the parton shower modelling, while the jet energy scale and resolution and the uncertainty related to the JVF cut result in a smaller bias.

Source i	Description	Impact $\Delta_i \rho / \rho$
Cluster Systematics	Energy Scale, Angular Resolution	2% – 10%
Pileup	Number of primary vertices	2% – 10%
Unfolding-Model	Parton shower modelling	1% – 8%
Jet Energy Scale	Uncertainty on the jet calibration	$\simeq 5\%$
Jet Energy Resolution	Calorimeter energy resolution σ	$\simeq 5\%$
JVF	JVF-related uncertainty	$< 1\%$

Table 1: Summary of the main sources of systematic uncertainties, together with their estimated impact

7. Results at the particle level

The results at the particle level are presented in Fig. 3 for the first p_T bin $30 \text{ GeV} < p_T < 40 \text{ GeV}$, together with the MC expectations from MC@NLO and POWHEG+PYTHIA. As expected, the observation that b -jets have a wider energy density distribution inside the jet cone holds for each p_T bin considered in the analysis.

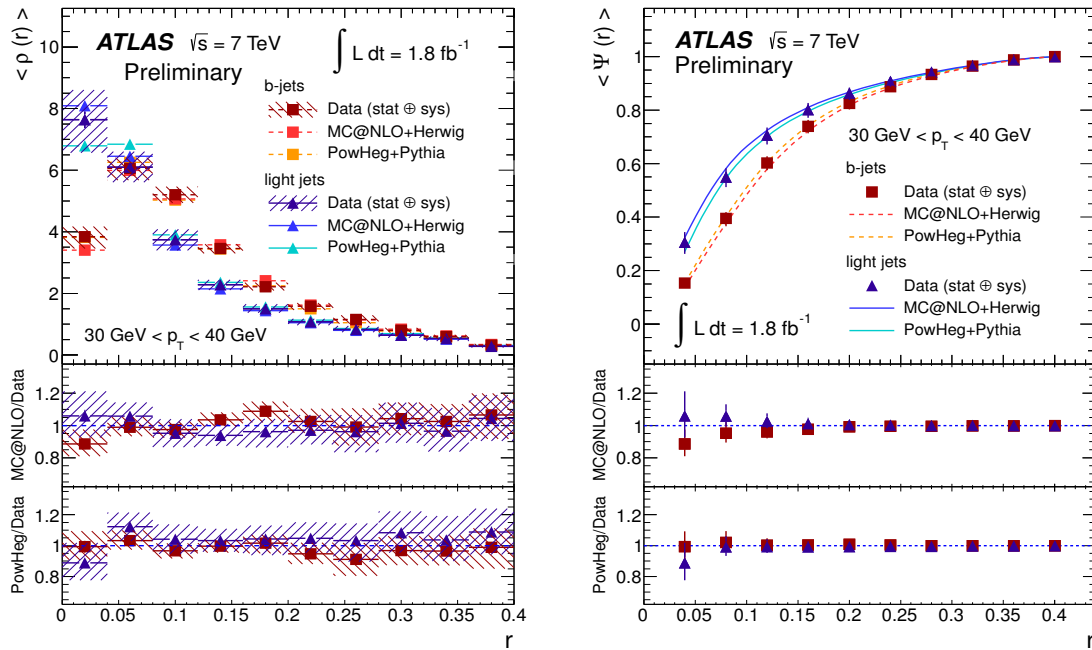


Figure 3: Unfolded values for $\langle \rho(r) \rangle$ (left) and $\langle \Psi(r) \rangle$ (right), together with statistical and systematic uncertainties for $30 \text{ GeV} < p_T < 40 \text{ GeV}$.

The unfolded results confirm the expectations that light-quark jets are narrower than those initiated by a b -quark. Monte Carlo studies have been carried out for the final state dependence of jet shapes, showing that quark-induced jets in the $t\bar{t}$ final state are narrower than quark-induced jets in inclusive jet production. This can be considered as an effect of the different colour flows in both processes.

References

- [1] S.D. Ellis, Z. Kunszt and D. Soper, Phys. Rev. Lett. **69**, 3615 (1992). arXiv:9208249 [hep-ph]
- [2] ATLAS Collaboration, Phys. Rev. D **83**, 052003 (2011). arXiv:1101.0070 [hep-ex]
- [3] CMS Collaboration, J. High Energy Phys. **06**, 160 (2012). arXiv:1204.3170 [hep-ex]
- [4] CDF Collaboration, A. Abulencia *et al.* Phys. Rev. D **78**, 072005 (2008). arXiv:0806.1699 [hep-ex]
- [5] ATLAS Collaboration, J. High Energy Phys. **1205** 059 (2012). arXiv:1202.4892 [hep-ex]
- [6] ATLAS Collaboration, Phys. Lett. B **711**, 244 (2012). arXiv:1201.1889 [hep-ex]
- [7] ATLAS Collaboration, ATLAS-CONF-2012-043. <http://cds.cern.ch/record/1435197>